buildings

MDPI

*Article*

# Study on Engineering Properties and Mechanism of Loess Muck Grouting Materials

**Zhenxu Wu [1], Chaoliang Ye [1,*], Benguo He [2], Fengxu Cao [1] and Tao Zhang [1]**

[1] School of Civil Engineering, Shijiazhuang Tiedao University, Shijiazhuang 050043, China; azwuzx@163.com (Z.W.); caofxu@stdu.edu.cn (F.C.); 1202201014@student.stdu.edu.cn (T.Z.)
[2] Key Laboratory of Ministry of Education on Safe Mining of Deep Metal Mines, Northeastern University, Shenyang 110819, China; hebenguo@mail.neu.edu.cn
* Correspondence: yechl@stdu.edu.cn

**Abstract:** Shield tunneling generates a massive amount of muck, and achieving the on-site reuse of muck is an urgent need in the field of shield tunneling. This study, based on a section of the Xianyang diversion tunnel in a loess stratum, aims to optimize the mix ratios of loess muck grouting materials to meet specific performance requirements. Laboratory tests were conducted to analyze the effects of the bentonite content and water–solid ratio on the properties of grout. The engineering properties, cost, and environmental impact of the optimized loess muck grouting materials were compared with those of traditional grouting materials. Additionally, XRD, SEM, and CT were employed to investigate the solidification mechanism of loess muck grouting materials. The results show that the bleeding rate, setting time, fluidity, and consistency of loess muck grouting materials decreased with increasing bentonite content, while these properties increased as the water–solid ratio rose. The compressive strength reached 0.26 MPa and 1.05 MPa at 3 d and 28 d, respectively. Compared to traditional grouting materials, the economic cost and carbon emissions of loess muck grouting materials were reduced by 49.46% and 37.17%, respectively. As the curing time increased, gel filling and particle agglomeration reduced the number of pores. The dense microstructure is the primary factor for the improvement of strength.

**Keywords:** shield tunneling; synchronous grouting; shield muck; microstructure

check for updates

**Citation:** Wu, Z.; Ye, C.; He, B.; Cao, F.; Zhang, T. Study on Engineering Properties and Mechanism of Loess Muck Grouting Materials. *Buildings* **2024**, *14*, 3400. https://doi.org/10.3390/buildings14113400

Academic Editor: Antonio Caggiano

Received: 19 September 2024
Revised: 19 October 2024
Accepted: 24 October 2024
Published: 25 October 2024

**Copyright:** © 2024 by the authors. Licensee MDPI, Basel, Switzerland. This article is an open access article distributed under the terms and conditions of the Creative Commons Attribution (CC BY) license (https://creativecommons.org/licenses/by/4.0/).

## 1. Introduction

Shield tunneling is widely used in tunnels, highways, and municipal pipelines due to its efficiency, and safety [1]. However, shield tunneling generates a substantial amount of muck [2]. It is estimated that over 225 million cubic meters of muck are produced annually from shield tunneling, with disposal costs reaching 58.2 billion RMB [3]. Current disposal methods primarily involve simple accumulation or landfilling [4,5]. The methods occupy large amounts of land. It also allows harmful substances from the shield muck to seep into the ground with rainfall [6]. Although existing studies have demonstrated that shield muck can be used to produce recycled aggregates [7,8], lightweight building materials [9,10], and filling materials [11,12], the resource utilization rate of shield muck in China remains below 1% [13]. Moreover, most of these processing methods still involve transporting shield muck, which results in higher handling costs, environmental concerns, and traffic safety issues [14]. Therefore, achieving the on-site reuse of shield muck is an urgent need in shield construction.

An annular gap forms between the segment and the surrounding ground due to the larger diameter of the shield cutterhead compared to the segment [15,16]. To reduce surface settlement and prevent segment displacement, grout is injected into the shield gap during tunneling [17,18], as shown in Figure 1. In recent years, the reuse of muck for preparing grouting materials has become a research hotspot, as it helps reduce the environmental impact of muck and the consumption of cement and river sand. The bentonite content

and water–solid ratio have a significant impact on the properties of muck grout. Luo et al. used XRD to analyze the composition of shield muck, bentonite, and river sand, confirming the feasibility of replacing bentonite and river sand with shield muck [19]. Miltiadou-Fezans and Zhang et al. found that the performance of muck grouting materials varies significantly with a change in the powder content (such as bentonite) and water–solid ratio. In addition, the fly ash–cement ratio and additive content also influenced the performance of grout [20,21]. Zhou investigated the properties of sandy muck grouting materials. He found that the initial setting time was longer compared to traditional grouting materials [22]. Cui et al. enhanced the properties of shield muck grouting materials by adding 0.02% epoxy resin and $SiO_2$, finding that shield muck grouting materials exhibited better stability compared to traditional grouting materials [23]. Ni et al. applied a multi-objective optimization method and found that the optimal performance could achieved [24]. Based on laboratory tests and field applications, Zhang et al. concluded that sandy muck grouting materials with appropriate mix ratios can meet construction requirements. The effectiveness of grout was further validated by the monitoring of surface settlement and segment uplift [4].

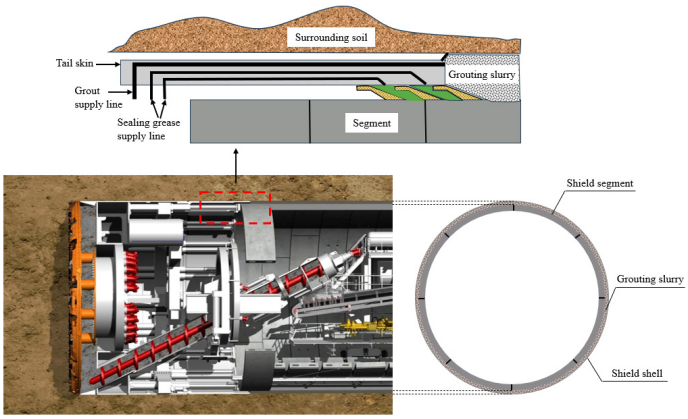



**Figure 1.** Synchronous grouting between segment lining and surrounding soil.

Loess particles are characterized by their small size, high clay content, and elevated moisture level. These characteristics significantly influence the performance of grouting materials. Compared to sandy muck, loess muck requires a more precisely optimized water–solid ratio and binder content to achieve adequate fluidity, filling ability, and strength of grout. Although some scholars have investigated the properties of sand muck grouting materials, the effects of bentonite and the water–solid ratio on the properties of grouting materials made from loess muck in shield tunneling are still unclear. Furthermore, the solidification mechanism of loess muck grouting materials (LMGMs) has not been comprehensively described. Additionally, there are few comparative studies between shield muck grouting materials and traditional grouting materials.

In this work, loess muck from the shield construction in the Xianyang section of the Hanjiang–Weihe River Project was used as a case study. Firstly, the fresh and mechanical properties of LMGMs with a different bentonite content and water–solid ratio were tested. The suitable mix ratios were recommended based on construction requirements. Subsequently, LMGMs with the optimal ratios were compared to traditional grouting materials in terms of their engineering properties, cost, and environmental influence. Finally, the solidification mechanism of LMGMs was investigated at a microscopic level by using XRD, SEM, and CT.

## 2. Experimental Program

### *2.1. Raw Materials*

The soil samples were obtained from a shield construction site in Xianyang City, Shanxi province, China. The excavated soil is composed of loess. The dry density, liquid limit, plastic

limit, and plasticity index of muck were 1.55 g/cm$^3$, 33.8%, 18.9%, and 14.9, respectively [25]. Figure 2 illustrates the particle size distribution of the soil samples. SEM and XRD tests were conducted on dried soil samples, and the results are shown in Figures 3 and 4. The soil structure is loose with large interparticle pores and point contact between particles. The size and shape of particles varied significantly. The mineral composition of the soil mainly includes quartz, muscovite, and feldspar, which are relatively stable. Therefore, from the perspective of mineral composition, loess muck can be considered a viable substitute for river sand.

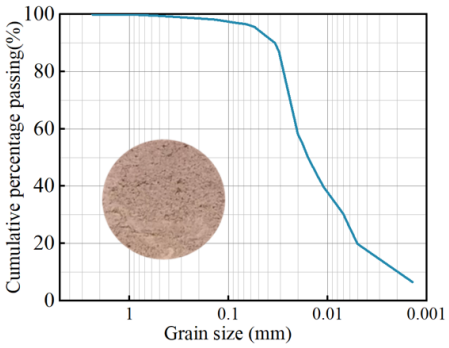



**Figure 2.** The particle size distribution.

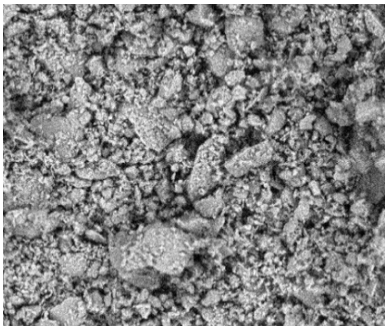


**Figure 3.** SEM image (×5000) of loess.

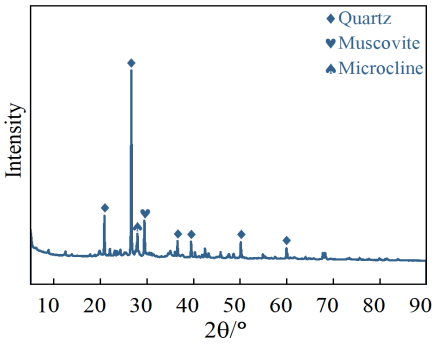



**Figure 4.** The XRD of loess.

Cement, fly ash, and calcium-based bentonite were procured from Shijiazhuang, Hebei province, China. The chemical compositions of cement and fly ash are presented in Table 1, while the physical properties of calcium-based bentonite are detailed in Table 2.

**Table 1.** Chemical composition of cement and fly ash.

| Material | $SiO_2$ | CaO | $Al_2O_3$ | $Fe_2O_3$ | MgO | $K_2O$ | $SO_3$ |
|---|---|---|---|---|---|---|---|
| Cement | 21.45% | 65.72% | 5.64% | 4.17% | 1.12% | 0.35% | 1.34% |
| Fly ash | 40% | 10% | 30% | 4.20% | 2.50% | 1.10% | 2.42% |

**Table 2.** Main physical property of bentonite.

| PH | Expansion Index (mL/2 g) | Expansion Capacity (mL/g) | Colloid Number (mL/15 g) | 2 h Water Absorption (%) | Moisture Content (%) | Granularity (%) |
|---|---|---|---|---|---|---|
| 9~9.5 | 20~22 | ≥50 | ≥400 | 200~250 | ≤12 | Pass 200-mesh ≥ 95% |

### *2.2. Mix Ratios and Preparation of LMGMs*

Loess muck has a high moisture content and a significant proportion of fine particles. They play a crucial role in designing mix ratios for grouting materials. The high moisture content necessitates precise control of water–solid ratio. Meanwhile, the higher fine particle content may improve the consolidation properties of LMGMs. Therefore, preliminary experiments are essential before designing the grouting materials mix.

To reduce costs and conserve natural resources, the bentonite content should not exceed that used in traditional grouting materials. The mix proportions of traditional grouting materials are shown in Table 3. The preliminary experiments primarily focused on the injectability (fluidity) and stability (bleeding rate) of LMGMs. Tests were conducted on LMGMs with 0% and 7% bentonite content under different water–solid ratio. The results showed that, with 0% bentonite content and a water–solid ratio of 0.46, the bleeding rate of LMGMs was excessively high (6.43%). Meanwhile, when the bentonite content was 7% and the water–solid ratio was 0.42, the fluidity of LMGMs was insufficient (156 mm). Therefore, the water–solid ratio for LMGMs was set between 0.42 and 0.46, with bentonite content ranging from 0% to 7%. The mix proportions are shown in Table 4.

**Table 3.** Mix ratio of traditional grouting materials.

| Control Group | Cement/% | Fly Ash/% | Bentonite/% | Sand/% | Water/Solid Ratio |
|---|---|---|---|---|---|
| | 13 | 22 | 7 | 58 | 0.33 |

**Table 4.** Mix ratios of LMGMs.

| NO. | Cement/% | Fly Ash/% | Muck/% | Bentonite/% | Water/Solid Ratio |
|---|---|---|---|---|---|
| 1 | 10 | 40 | 50 | 0 | 0.42 |
| 2 | 10 | 40 | 50 | 0 | 0.44 |
| 3 | 10 | 40 | 50 | 0 | 0.46 |
| 4 | 10 | 40 | 50 | 3 | 0.42 |
| 5 | 10 | 40 | 50 | 3 | 0.44 |
| 6 | 10 | 40 | 50 | 3 | 0.46 |
| 7 | 10 | 40 | 50 | 7 | 0.42 |
| 8 | 10 | 40 | 50 | 7 | 0.44 |
| 9 | 10 | 40 | 50 | 7 | 0.46 |

The muck was dried and crushed, then sieved through a 5 mm mesh before preparing the LMGMs. A QJ-20 brick mixer was used for the preparation, as illustrated in Figure 5. First, measured quantities of cement, fly ash, bentonite, and muck were added to the mixing pot and dry-mixed for 3 min. Water was then added, and the mixture was blended for 4 min to form LMGMs. The fresh properties of the slurry were tested immediately after mixing. Subsequently, the slurry was poured into 50 × 50 mm cylindrical mold to measure the hardening properties of LMGMs. The samples in the mold were placed in a curing chamber and demolded after 24 h. The demolded samples were returned to the curing chamber for further curing until the testing age was reached.

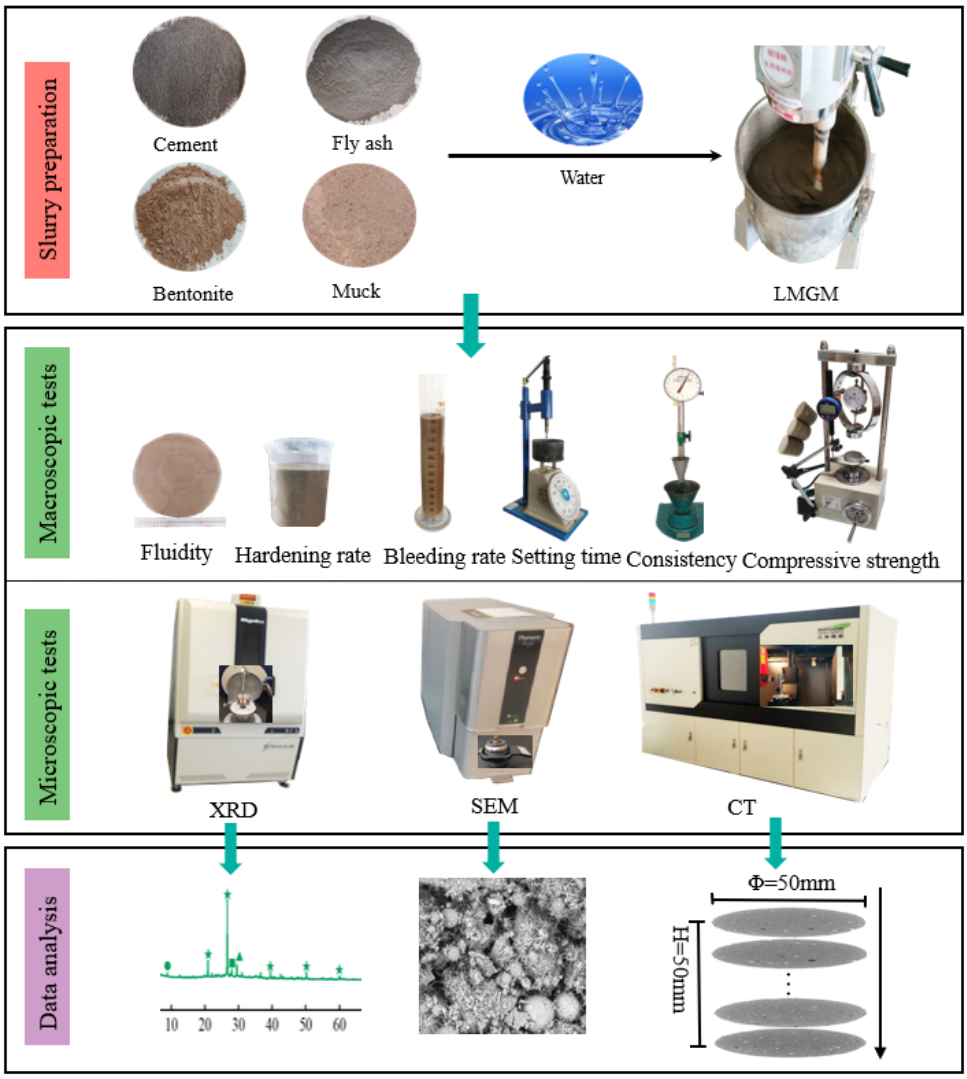



**Figure 5.** The preparation and testing procedure flowchart for LMGMs.

### *2.3. Test Items*

The test items for LMGMs are shown in Figure 5.

The fresh properties of LMGMs were assessed by measuring bleeding rate, setting time, fluidity, and consistency. The bleeding rate was tested according to the Technical Specification for Simultaneous Grouting Material in Shield Projects [26]. Setting time and consistency were tested according to the Standard for Test Method of Basic Properties of Construction Mortar [27]. Setting time was measured by using a ZKS-100 setting time tester (Zhongjiaojianyi, Beijing, China) through penetration resistance method. Consistency was measured with a mortar consistency tester. Fluidity was tested according to the Technical Code for Application of Cementitious Grout. Additionally, based on practical engineering requirements, the grouting materials need to be injected into the shield tail gap within 0 to 3 h after preparation [28]. Therefore, the fluidity of LMGMs was tested at hourly intervals, with the grout re-mixed for 120 s before each test.

The test indicators for hardening properties included hardening rate and compressive strength. The hardening rate was tested according to the Technical Specification for Simultaneous Grouting Material in Shield Projects [26]. The slurry was poured into 500 mL beaker. After resting for 1 min, the initial volume of slurry was recorded. The hardening rate was determined as the ratio of the grout volume after 3 d to its initial volume. The compressive strength was tested according to the Test Methods of Materials Stabilized with Inorganic Binders for Highway Engineering [29]. The compressive strength of LMGMs

was tested using the YYW-II unconfined pressure apparatus at a loading rate of 1 mm/min. In this study, samples were tested at curing ages of 12 h, 1 d, 3 d, 7 d, and 28 d. For each mix ratio of LMGMs, three parallel samples were tested, and their average value was used as the result.

XRD, SEM, and CT were employed to analyze the microstructure of LMGMs. The mineral composition for LMGMs was determined through XRD analysis. Sample was dried, ground to less than 75 μm, and scanned at a rate of 5°/min over a range of 5~90°. SEM was used to observe the microstructure and mineral morphology of LMGMs. The pore characteristics of LMGMs were investigated by using CT. The test sample was 50 × 50 mm cylinder, with a resolution of 27.34 μm and a scan time of 1200 s. The sample was divided into multiple vertical cross-sectional slices through CT scanning, which were reconstructed into a 3D model. This 3D model enabled the analysis of internal defects and pore structures within the sample.

### *2.4. Performance Requirements*

Grouting materials should maintain adequate fluidity for a sufficient duration to ensure that the slurry can fully fill the shield gap after pumping. The setting time must also be appropriate: if it is too short, it may cause pipe blockages, whereas, if it is too long, it can lead to slurry loss [30]. Grouting materials must exhibit good volumetric stability after injection to prevent static segregation. Once hardened, they should attain sufficient early strength and appropriate long-term strength to resist surrounding soil pressure. This study focuses on shield tunneling in loess, where the compressive strength of undisturbed soil is 0.11 MPa. Therefore, based on the standard and construction conditions [26], grouting materials for this project must meet the requirements listed in Table 5.

**Table 5.** Construction requirements of LMGMs.

| Item | Bleeding Rate/% | Setting Time/h | Fluidity /mm | Consistency /cm | Hardening Rate/% | Compressive Strength/MPa | |
|---|---|---|---|---|---|---|---|
| | | | | | | 3/d | 28/d |
| Requirements | <5 | 10~24 | >160 | 11–16 | >95 | 0.15 | 1 |

## 3. Results and Discussion

### *3.1. Fresh Properties*

#### 3.1.1. Bleeding Rate

Figure 6 shows the influence of bentonite and the water–solid ratio on the bleeding rate of LMGMs. Except for NO.3 (10% for cement, 40% for fly ash, 50% for muck, 0% for bentonite, and 0.46 for the water–solid ratio) and NO.6 (10% for cement, 40% for fly ash, 50% for muck, 3% for bentonite, and 0.46 for the water–solid ratio), the bleeding rate of the other LMGMs was less than 5%. At the same water–solid ratio, the bleeding rate of LMGMs decreased with the increase in bentonite content [31]. When the bentonite content increased from 0% to 7%, the bleeding rate for LMGMs with a water–solid ratio of 0.42, 0.44, and 0.46 decreased from 4.09%, 4.12%, and 6.43% to 0.82%, 1.85%, and 4.1%, representing reductions of 79.95%, 55.1%, and 36.24%, respectively. This reduction may be attributed to the strong water absorption capacity of bentonite. As the bentonite content increases, more water molecules are absorbed within the slurry, which significantly increases the viscosity between loess particles and enhances the slurry stability, thereby reducing the bleeding rate. At the same bentonite, the bleeding rate of LMGMs rose as the water–solid ratio increased. As the water–solid ratio rose from 0.42 to 0.46, the bleeding rate of LMGMs with a bentonite content of 0%, 3%, and 7% increased from 4.09%, 1.61%, and 0.82% to 6.43%, 5.79%, and 4.10%, representing increases of 57.21%, 295%, and 400%, respectively. This is attributed to the higher water–solid ratio in LMGMs, which results in an increase in the unreacted free water content [32].

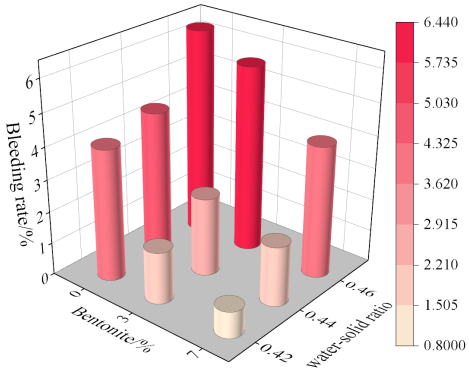



**Figure 6.** Bleeding rate test results of LMGMs.

### 3.1.2. Setting Time

Figure 7 illustrates the influence of the bentonite content and water–solid ratio on the setting time of LMGMs. It could be adjusted from 12 to 18.7 h by altering these factors, with NO.7 (10% for cement, 40% for fly ash, 50% for muck, 7% for bentonite, and 0.42 for the water–solid ratio) having the shortest setting time and NO.3 having the longest. At the same water–solid ratio, the setting time decreased as the bentonite content increased. When the bentonite content increased from 0% to 7%, the setting time of LMGMs with a water–solid ratio of 0.42, 0.44, and 0.46 decreased from 15.8 h, 16 h, and 18.7 h to 12 h, 12.7 h, and 14.3 h, representing reductions of 24.05%, 20.63%, and 23.53%, respectively. This is because increased bentonite absorbs excess free water, accelerating gel formation and shortening the setting time [33]. At a fixed bentonite content, the setting time increased as the water–solid ratio rose, which is consistent with Lisa's finding [34]. As the water–solid ratio increased from 0.42 to 0.46, the setting time of LMGMs with a bentonite content of 0%, 3%, and 7% increased from 15.8 h, 13 h, and 12 h to 18.7 h, 17.2 h, and 14.3 h, representing increases of 18.35%, 32.31%, and 19.17%, respectively. This is because, as the water–solid ratio increases, the distance between particles within LMGMs also increases, which slows down the rate of gel formation from cement hydration. Consequently, it prolongs the formation time of the LMGMs network structure [35].

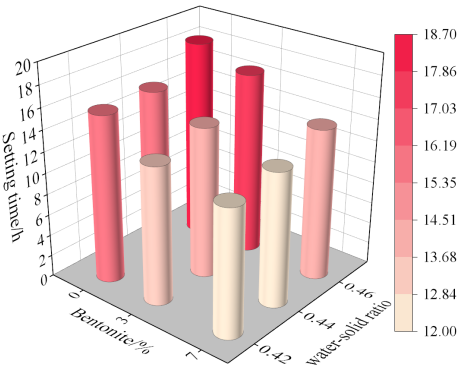



**Figure 7.** Setting time test results of LMGMs.

### 3.1.3. Fluidity

Figure 8 illustrates the influence of bentonite and the water–solid ratio on the fluidity of LMGMs and its loss over time. The initial fluidity could be adjusted from 156 to 282 mm by altering these factors, with NO.7 having the lowest initial fluidity and NO.3 having the highest. At a constant water–solid ratio, the initial fluidity decreased as bentonite increased [36]. When the bentonite content increased from 0% to 7%, the initial fluidity of LMGMs with a water–solid ratio of 0.42, 0.44, and 0.46 decreased from 225, 255, and 282 mm to 156, 205, and 225 mm, representing reductions of 30.67%, 19.61%, and 20.21%, respectively. Conversely, at the same bentonite, the initial fluidity increased

as the water–solid ratio increased. As the water–solid ratio increased from 0.42 to 0.46, the initial fluidity of LMGMs with a bentonite content of 0%, 3%, and 7% increased from 225, 193, and 156 mm to 282, 277, and 225 mm, representing increases of 25.33%, 43.52%, and 44.23%, respectively. These results are linked to the amount of free water within the grout. The increased bentonite absorbs a significant amount of free water, enhancing the friction between particles, which leads to a decrease in LMGMs fluidity. Conversely, as the water rises, more water molecules in LMGMs reduce particle friction, resulting in increased fluidity [37].

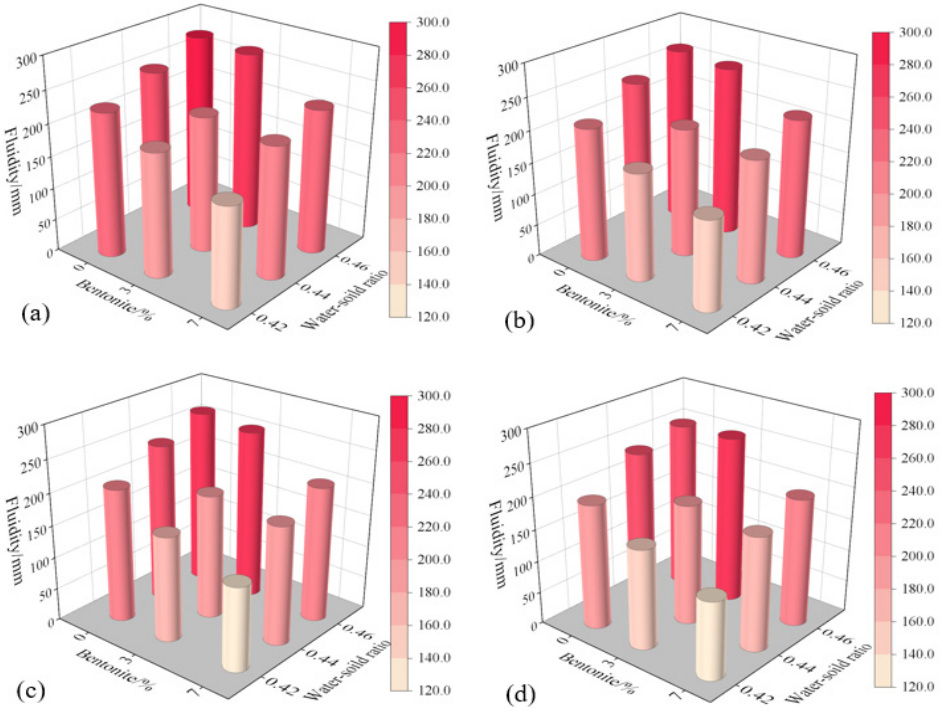



**Figure 8.** Fluidity test results of LMGMs: (**a**) initial; (**b**) 1 h; (**c**) 2 h; and (**d**) 3 h.

The fluidity of LMGMs decreased over time. When the fluidity is greater than 160 mm, the slurry is pumpable [26]. The fluidity of NO.1~NO.3, NO.5, NO.6, NO.8, and NO.9 ranged from 178 mm to 260 mm at 3 h. The loss of fluidity over time was amplified by the higher bentonite content. At a water–solid ratio of 0.42, the fluidity of LMGMs with 3% bentonite decreased from 193 mm to 156 mm within 3 h. This reduction in fluidity made the slurry unpumpable. The fluidity of LMGMs with 0% bentonite decreased from 225 mm to 195 mm within 3 h, and the slurry remained pumpable. This is because the increased bentonite absorbs a significant amount of free water molecules in LMGMs [38]. It accelerates the rate of cement hydration and gel formation, thereby increasing the rate of fluidity loss over time. Conversely, the loss of fluidity over time decreased as the water–solid ratio rose. When the bentonite content was 3%, the fluidity of LMGMs with a water–solid ratio of 0.42 decreased from 193 to 156 mm, while the fluidity of LMGMs with a water–solid ratio of 0.46 decreased from 277 mm to 260 mm within the same time period. This is because an increased water–solid ratio inhibits the cement hydration reaction, thereby slowing down the rate of fluidity loss over time in LMGMs [39].

### 3.1.4. Consistency

Figure 9 illustrates the influence of bentonite and the water–solid ratio on the consistency of LMGMs and its loss over time. The initial consistency could be adjusted from 13.6 to 17 cm by altering these factors, with NO.7 having the lowest initial consistency and NO.3 having the highest. Under the same water–solid ratio, the initial consistency of LMGMs decreased as the bentonite rose. As the bentonite increased from 0% to 7%, the

initial consistency of LMGMs with a water–solid ratio of 0.42, 0.44, and 0.46 decreased from 15.1 cm, 16.1 cm, and 17 cm to 13.6 cm, 15.1 cm, and 15.3 cm, representing reductions of 9.93%, 6.21%, and 10%, respectively. Conversely, under the same bentonite, the initial consistency of LMGMs increased as the water–solid ratio increased. When the water–solid ratio increased from 0.42 to 0.46, the initial consistency of LMGMs with a bentonite content of 0%, 3%, and 7% increased from 15.1, 13.9, and 13.6 cm to 17, 16.1, and 15.3 cm, representing increases of 12.58%, 15.83%, and 12.5%, respectively.

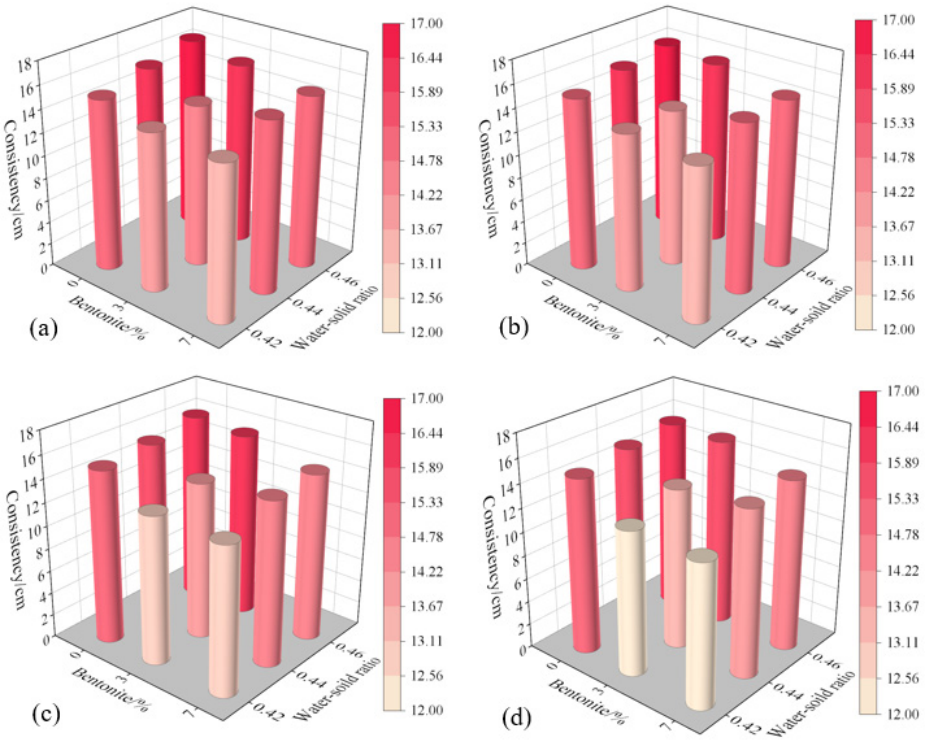



**Figure 9.** Consistency test results of LMGMs: (**a**) initial; (**b**) 1 h; (**c**) 2 h; and (**d**) 3 h.

The consistency of LMGMs decreased over time. The consistency of NO.1, NO.4, NO.5, NO.7, NO.8, and NO.9 ranged from 12 cm to 14.8 cm at 3 h. The loss of consistency over time increased as the bentonite rose. When the water–solid ratio was 0.44, the consistency of LMGMs with 0% bentonite decreased from 16.1 cm to 15.5 cm within 3 h, while the consistency of LMGMs with 7% bentonite decreased from 15.1 cm to 14.1 cm within 3 h. Conversely, the loss of consistency over time decreased as the water–solid ratio rose. When bentonite was 3%, the consistency of LMGMs with a water–solid ratio of 0.42 decreased from 13.9 cm to 12.2 cm within 3 h, while the consistency of LMGMs with a water–solid ratio of 0.46 decreased from 16.1 cm to 15.8 cm within 3 h.

### *3.2. Hardening Properties*

#### 3.2.1. Hardening Rate

The influence of bentonite and the water–solid ratio on the hardening rate of LMGMs is shown in Figure 10. The hardening rate of LMGMs could be adjusted from 86.5 to 99% by altering these factors, with NO.3 (10% for cement, 40% for fly ash, 50% for muck, 0% for bentonite, and 0.46 for the water–solid ratio) having the lowest hardening rate and NO.7 (10% for cement, 40% for fly ash, 50% for muck, 0% for bentonite, and 0.46 for the water–solid ratio) having the highest. The hardening rate of LMGMs increased as the bentonite rose. When the bentonite content rose from 0% to 7%, the hardening rate of LMGMs with a water–solid ratio of 0.42, 0.44, and 0.46 increased from 96%, 94.5%, and 86.5% to 99%, 97.5%, and 92%, representing increases of 3.13%, 3.17%, and 6.36%, respectively. Conversely, at the same bentonite, the hardening rate of LMGMs decreased as the water–solid ratio rose. As

the water–solid ratio rose from 0.42 to 0.46, the hardening rate of LMGMs with bentonite content of 0%, 3%, and 7% decreased from 96%, 96.6%, and 99% to 86.5%, 91.2%, and 92%, representing reductions of 9.9%, 5.59%, and 7.61%, respectively.

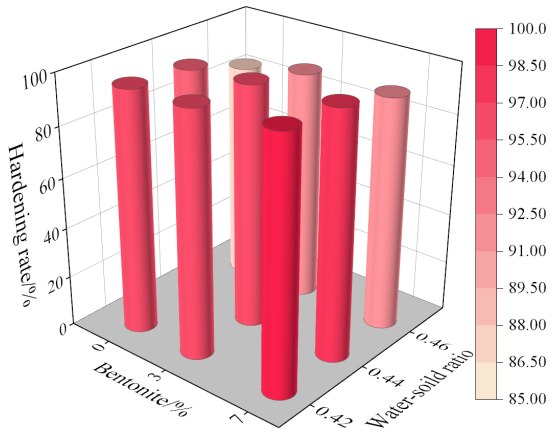



**Figure 10.** Hardening rate test results of LMGMs.

### 3.2.2. Compressive Strength

Figure 11 illustrates the effects of bentonite and the water–solid ratio on the compressive strength of LMGMs. By adjusting the mix ratios, the compressive strength after curing for 12 h, 1, 3, 7, and 28 d was 0.02~0.04 MPa, 0.08~0.13 MPa, 0.19~0.3 MPa, 0.37~0.51 MPa, and 0.73~1.15 MPa, respectively. The compressive strength of LMGMs increased gradually with curing time. At early curing stages, differences in mix ratios had minimal effect. However, as the curing time increased, the variations in compressive strength became more pronounced. The compressive strength of LMGMs cured for 28 d initially increased and then decreased as the bentonite rose. With 3% bentonite, the compressive strength of LMGMs at a water–solid ratio of 0.42, 0.44, and 0.46 was 9.52%, 17.44%, and 8.22% higher, respectively, compared to LMGMs without bentonite. Conversely, with 7% bentonite, the compressive strength at the same ratios was 9.52%, 6.98%, and 2.67% lower than LMGMs without bentonite. The reason is that an appropriate amount of bentonite can improve the uniformity of grout, enhancing the bonding strength between muck particles and increasing the density of the internal structure, which, in turn, raises the compressive strength. However, when the bentonite content is too high, its water absorption capacity can lead to insufficient cement hydration, resulting in more pores and reduced compactness, thereby decreasing the compressive strength. The compressive strength of LMGMs decreased as the water–solid ratio increased. When the ratio rose from 0.42 to 0.46, the compressive strength with 0%, 3%, and 7% bentonite dropped by 30.47%, 31.30%, and 21.05%, respectively. This shows that a higher water–solid ratio significantly reduces LMGMs strength [40]. The reason is that an increase in the water–solid ratio prevents gel products generated by the cement hydration reaction from forming a complete network structure. This leads to the formation of more pores during the hardening process of LMGMs, resulting in a loose internal structure and reduced compressive strength after solidification [41].

By testing various indicators of LMGMs, it was found that NO.1 (10% for cement, 40% for fly ash, 50% for muck, 0% for bentonite, and 0.42 for the water–solid ratio) and NO.5 (10% for cement, 40% for fly ash, 50% for muck, 3% for bentonite, and 0.44 for the water–solid ratio) meet the on-site construction requirements. The relevant indicators are shown in Table 6. Bentonite is not only expensive but also a non-renewable resource. To align with the national sustainable development goal and reduce costs, its use should be minimized. Consequently, NO.1 is recommended for synchronous grouting in shield tunneling.

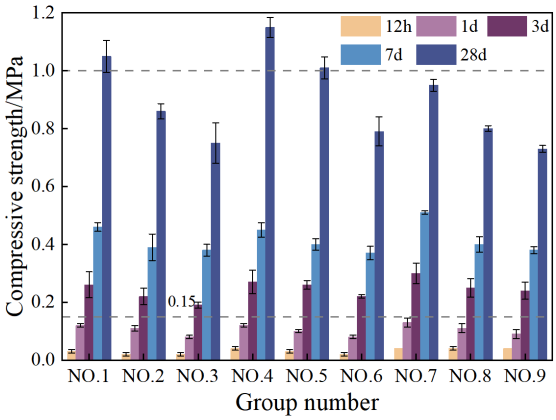



**Figure 11.** Compressive strength test results of LMGMs.

**Table 6.** The performance indicators of NO.1 and NO.5.

| NO. | Bleeding Rate/% | Hardening Rate/% | Setting Time/h | Fluidity/mm | Consistency/cm | Compressive Strength/MPa | |
|---|---|---|---|---|---|---|---|
| | | | | | | 3 d | 28 d |
| NO.1 | 4.09 | 96 | 15.8 | 195 | 14.8 | 0.22 | 1.05 |
| NO.5 | 2.44 | 96 | 13 | 188 | 13.6 | 0.22 | 1 |

To investigate the variation patterns in LMGMs performance with changes in the bentonite content and water–solid ratio, a multiple linear regression analysis was conducted. The fitting equations and corresponding results are presented in Table 7.

**Table 7.** Evaluation of fitting performance.

| Variable | Expression | $R^2$ | *p* |
|---|---|---|---|
| $f_{\text{bleeding rate}}$ | $-31.131 - 38.6X_1 + 81.667X_2$ | 0.896 | 0.001 |
| $f_{\text{setting time}}$ | $-17.768 - 54.279X_1 + 78.333X_2$ | 0.929 | <0.001 |
| $f_{\text{3-h fluidity}}$ | $-671.216 - 930.18X_1 + 2050X_2$ | 0.939 | <0.001 |
| $f_{\text{hardening rate}}$ | $172.869 + 53.919X_1 - 182.5X_2$ | 0.852 | 0.003 |
| $f_{\text{3-d strength}}$ | $0.887 + 0.559X_1 - 1.5X_2$ | 0.915 | <0.001 |
| $f_{\text{28-d strength}}$ | $4.16 - 1.023X_1 - 7.333X_2$ | 0.815 | 0.01 |

Note: $X_1$—bentonite content; $X_2$—water–solid ratio.

As shown in Table 7, the regression coefficients for both the dependent variables and independent variables are relatively high, indicating a strong correlation between LMGMs performance indicators and bentonite content as well as water–solid ratio. The significance level (*p*) is less than 0.05, demonstrating that the fitting results are statistically significant.

### *3.3. Comparative Analysis of Grouting Materials*

Figure 12 illustrates the performance of NO.1 (10% for cement, 40% for fly ash, 50% for muck, 0% for bentonite, and 0.42 for the water–solid ratio) compared to traditional grouting materials. NO.1 showed a 17.71% reduction in setting time, which was beneficial for improving the efficiency of shield construction. Its bleeding rate decreased by 16.87%, while the hardening rate increased by 1.01%, demonstrating improved stability and filling performance. Although the fluidity and compressive strength of NO.1 were lower than those of traditional grouting materials, the slurry still maintained adequate fluidity (195 mm) at 3 h. Moreover, its compressive strength at 28 d was 855% higher than that of the surrounding tunnel rock (0.11 MPa). Therefore, NO.1 is a grouting material with good injectability, high filling performance, and the ability to control the deformation of the loess stratum surrounding rock.

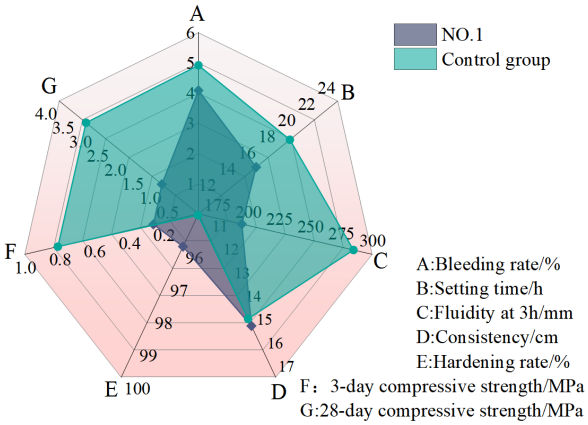



**Figure 12.** Performance of NO.1 and traditional grouting materials.

The cost of raw materials and preparation for 1 $m^3$ of NO.1 and the traditional grouting materials are listed in Table 8. Compared to traditional grouting materials, the cost of preparing 1 $m^3$ NO.1 was reduced by 128.8 RMB, resulting in cost savings of 49.46%. Therefore, LMGMs demonstrate a significant economic benefit. According to the relevant literature [23], the $CO_2$ emissions from raw materials and the preparation of 1 $m^3$ of NO.1 and traditional grouting materials are detailed in Table 8. Compared to traditional grouting materials, the preparation for 1 $m^3$ NO.1 reduced $CO_2$ emissions by 65.9 kg, representing a 37.17% decrease in carbon emissions. This reduction helps mitigate the environmental impact caused by the accumulation and transportation of shield muck. Therefore, LMGMs also demonstrate a significant environmental benefit.

**Table 8.** Cost and carbon emissions of NO.1 and control group.

| Main Projects | Price Comparison | | | Carbon Emission Comparison | | |
|---|---|---|---|---|---|---|
| | Market Price | Traditional Grouting Materials ($m^3$) | NO.1 ($m^3$) | Carbon Emission | Traditional Grouting Materials ($m^3$) | NO.1 ($m^3$) |
| Cement | 380 RMB/t | 180 kg | 121.8 kg | 94 0 kg/t | 180 kg | 121.8 kg |
| Fly ash | 175 RMB/t | 320 kg | 487.3 kg | — | 320 kg | 487.3 kg |
| River sand | 120 RMB/t | 800 kg | — | 5 kg/t | 800 kg | 0 |
| Bentonite | 400 RMB/t | 100 kg | — | 41 kg/t | 100 kg | 0 |
| Shield muck | — | — | 609.2 kg | −5.07 kg/t | — | 609.2 kg |
| Total | | 260.4 RMB | 131.6 RMB | | 177.3 kg | 111.4 kg |
| Savings | | | 128.8 RMB | | | 65.9 kg |

Additionally, a comparison between NO.1 and high-performance grouting materials is shown in Table 9 [32]. Although the performance of high-performance grouting materials was superior to LMGMs, the cost was increased by 298.1 RMB, making it impractical for real-world applications.

**Table 9.** The performance and cost for 1 $m^3$ of NO.1 and high-performance grouting materials.

| Group Number | Cost /RMB | Bleeding Rate/% | Hardening Rate/% | Setting Time/h | Fluidity /mm | Consistency /cm | Compressive Strength/MPa | |
|---|---|---|---|---|---|---|---|---|
| | | | | | | | 3 d | 28 d |
| NO.1 | 131.6 | 4.09 | 96 | 15.8 | 195 | 14.8 | 0.22 | 1.05 |
| high-performance grouting materials | 429.7 | 2.2 | — | 7.25 | 337 | — | 4.95 | 16.44 |

### *3.4. Microstructure Characteristics*

#### 3.4.1. XRD

The changes in the phase characteristic of LMGMs over different curing periods were investigated by conducting an XRD test on NO.1 (10% for cement, 40% for fly ash, 50% for muck, 0% for bentonite, and 0.42 for the water–solid ratio). The results are presented in Figure 13. NO.1 exhibited similar phase compositions across different curing periods. The identified phases included ettringite (AFt), calcium carbonate ($CaCO_3$), silicon dioxide ($SiO_2$), and calcium aluminosilicate hydrate ($CaAl_2Si_2O_8{\cdot}4H_2O$). AFt is an essential product of cement hydration, while $SiO_2$ and $CaAl_2Si_2O_8{\cdot}4H_2O$ mainly originate from the fly ash and muck. Comparing the X-ray diffraction patterns of NO.1 at different curing ages, it is evident that the intensity of the $SiO_2$ diffraction peak gradually decreased as the curing period extended. This indicates that the reactive $SiO_2$ in fly ash reacted with $Ca(OH)_2$ to form C-S-H gel, which filled the internal pores of LMGMs, thereby promoting the hardening process [42]. Additionally, as the reaction progressed, $SiO_2$ was gradually consumed, leading to a decrease in its diffraction peak intensity. The diffraction peaks of AFt and $CaCO_3$ in NO.1 increased significantly as the curing period extended [43], indicating that the cement hydration reaction continued over time and generated more AFt, $Ca(OH)_2$, and C-S-H gel. The gradual increase in $CaCO_3$ is attributed to the reaction between $Ca(OH)_2$ and carbonates present in the muck.

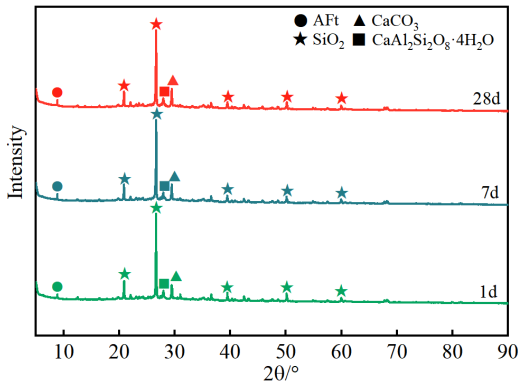



**Figure 13.** XRD results of NO.1.

Notably, the XRD of NO. 1 did not show any diffraction peak for $Ca(OH)_2$. This could be due to the following reasons: (1) the pozzolanic reaction between $Ca(OH)_2$ and the reactive $SiO_2$ and $Al_2O_3$ in fly ash reduces the $Ca(OH)_2$ content; and (2) the carbonates present in muck react with $Ca(OH)_2$ to form $CaCO_3$.

#### 3.4.2. SEM

Figure 14 shows the SEM images of NO.1 at different curing stages. NO.1 cured for 1 d displayed a range of particle sizes, with unhydrated fly ash (FA) primarily appearing as individual particles. This suggests that the hydration reactions of cement and fly ash had not fully progressed in the early stage. The particles in NO.1 were mostly in point contact with small contact areas, resulting in a loose structure with numerous pores. The limited formation of gel substances led to weak bonding between particles, contributing to the low strength of NO.1.

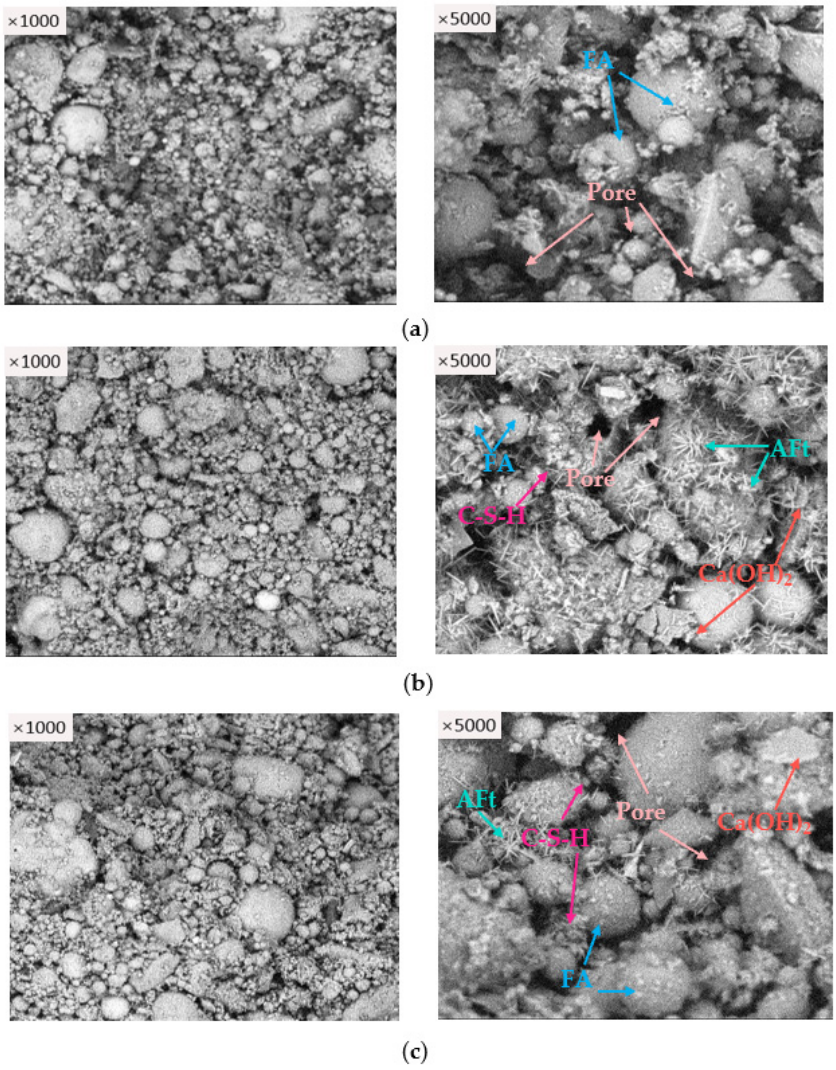
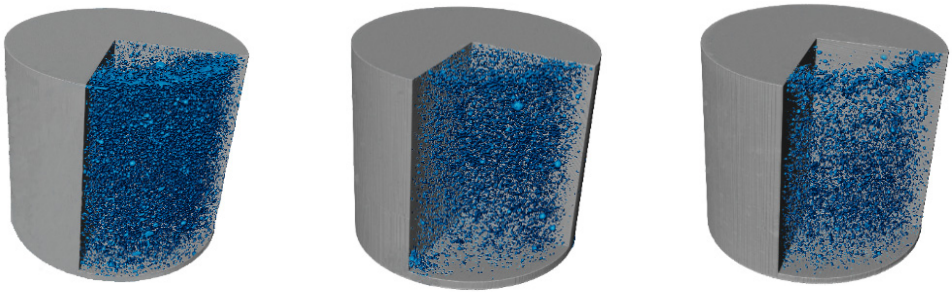



**Figure 14.** SEM images of NO.1: (**a**) 1 d; (**b**) 7 d; and (**c**) 28 d.

As the curing period increased, hydration reactions in NO.1 progressed and generated a significant amount of $Ca(OH)_2$, AFt, and C-S-H gel [44]. These gels filled the pores, which increased the contact area between particles and bonded them into a continuous cohesive matrix. The formation of C-S-H gel notably enhanced the density and strength of NO.1 [45]. Furthermore, ion exchange reactions occurred within the grout in the alkaline environment. This strengthened the electrostatic attraction between soil particles, leading to the formation of larger particle agglomerates. This rearrangement and bonding process further increased the compressive strength of LMGMs. As the curing continued, the filling action of gels and particle agglomeration reduced pore spaces within the LMGMs. This significantly improved the internal pore structure of LMGMs and gradually enhanced compressive strength, consistent with the analysis result in Figure 11.

### 3.4.3. CT

The 3D reconstruction results of NO.1′s pores are shown in Figure 15. NO.1 cured for 1 d exhibited a significant number of internal pores with large volumes. The largest pore measured 198.95 $mm^3$. As the curing period extended, the internal pores in the sample gradually decreased, and the pore volume diminished. The largest pore volumes in the sample cured for 28 d was reduced to 7.83 $mm^3$.



(**a**) (**b**) (**c**)

**Figure 15.** Three-dimensional recomposition of NO.1: (**a**) 1 d; (**b**) 7 d; and (**c**) 28 d.

To further analyze the evolution of pore characteristics in NO.1 over the curing period, a statistical analysis was conducted on the number and size distribution of the pores. Based on the pore size, pores with an equivalent diameter of less than 200 μm, 200~400 μm, 400~600 μm, and greater than 600 μm were defined as small pores, medium pores, large pores, and extra-large pores, respectively [46]. The distribution of these pores in the sample is shown in Figure 16, while the number and size distribution of the pores are presented in Figure 17. Pores of all sizes were uniformly distributed in the sample. The small pores were more abundant at each curing stage. The number of pores of all sizes decreased as the curing period extended. NO.1 cured for 1 d, 7 d, and 28 d had the highest number of pores in the 100~200 μm range, with counts of 48,105, 35,647, and 25,541, respectively. The proportion of small pores and medium pores increased with a longer curing time. The proportion of small pores in NO.1 at 1 d, 7 d, and 28 d was 47.08%, 50.42%, and 53.51%, respectively.

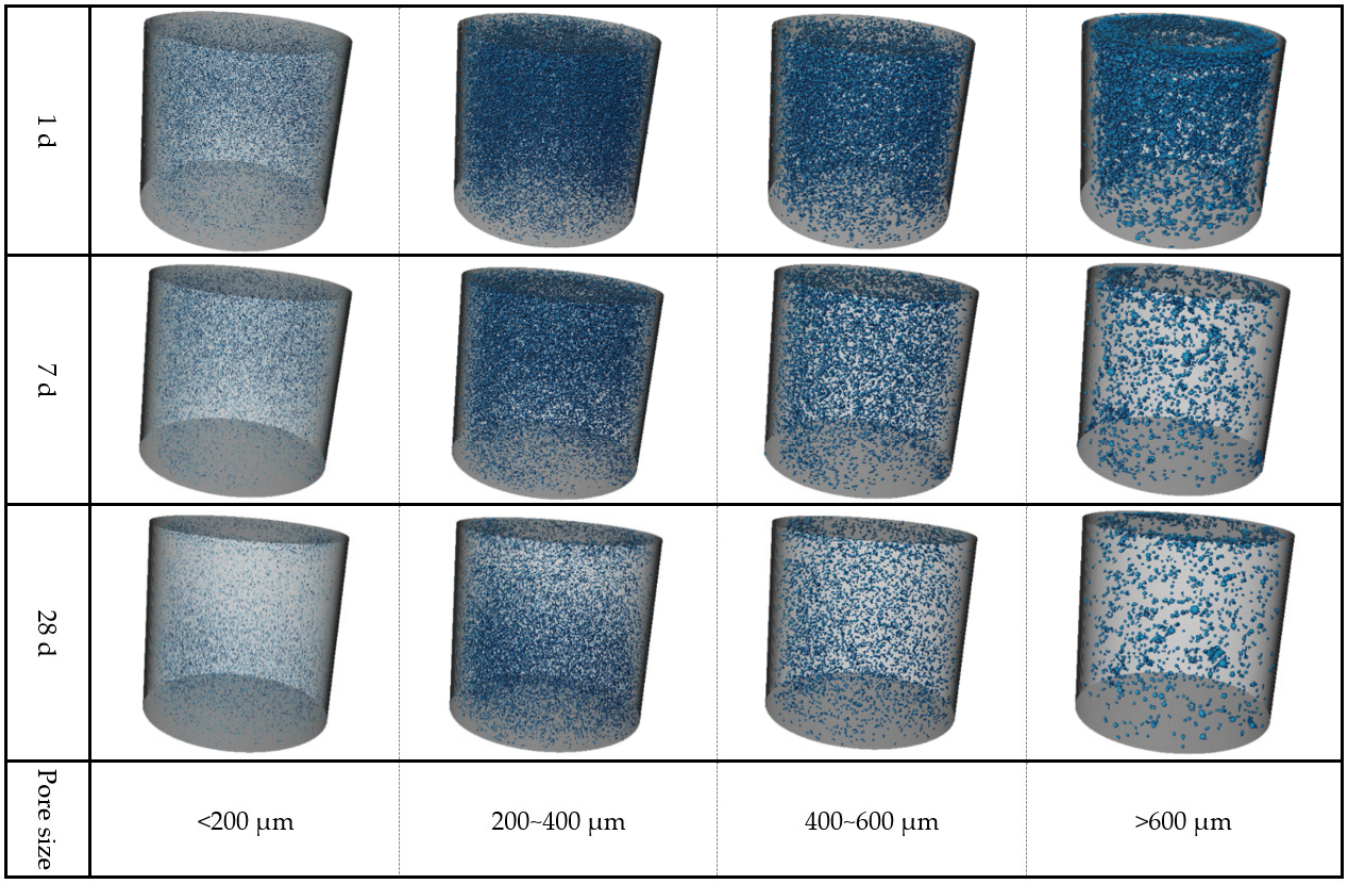



**Figure 16.** The 3-D pore structure of NO.1.

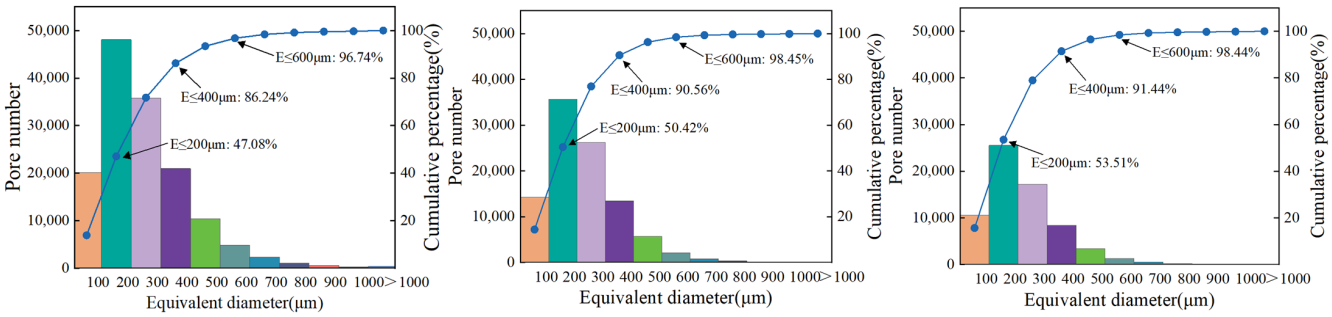



**Figure 17.** The pore characteristics of NO.1: (**a**) 1 d; (**b**) 7 d; and (**c**) 28 d.

In summary, as the curing time increases, gel filling and particle aggregation reduce the number of pores. This process transforms large pores into small ones in NO.1 [47]. Consequently, the internal structure of NO.1 becomes denser, leading to increased compressive strength. This finding is consistent with the results shown in Figure 11.

## 4. Conclusions

This study utilized loess muck from shield tunneling to prepare synchronous grouting materials. Based on laboratory experiments, a systematic analysis was conducted to evaluate the effects of the water–solid ratio and bentonite on LMGMs. Suitable mix ratios were recommended according to construction requirements, and a comparative analysis was conducted with traditional grouting materials in terms of the engineering properties, cost, and environmental impact. Additionally, XRD, SEM, and CT were employed to investigate the solidification mechanism of LMGMs. The main experimental conclusions are as follows:

(1) The bleeding rate, setting time, fluidity, and consistency of LMGMs decreased by 36.24~79.95%, 20.63~24.05%, 19.61~30.67%, and 6.21~10%, respectively, as the bentonite content increased from 0% to 7%. Conversely, these parameters increased by 57.21~400%, 18.35~32.31%, 25.33~44.23%, and 12.5~15.83% as the water–solid ratio rose from 0.42 to 0.46. Additionally, the hardening rate of LMGMs increased by 5.59~9.9% with a higher bentonite content but decreased by 3.13~6.36% as the water–solid ratio increased.

(2) The compressive strength of LMGMs initially increased and then decreased as the bentonite content increased, while it consistently decreased as the water–solid ratio rose. The compressive strength of LMGMs cured for 28 d reached 1.05 MPa, which was 855% higher than that of the tunnel surrounding rock.

(3) The performance of NO.1 (10% for cement, 40% for fly ash, 50% for muck, and 0.42 for the water–solid ratio) meets on-site construction requirements. Compared to traditional grouting materials, NO.1 reduced costs by 49.46% and carbon emissions by 37.17%, demonstrating significant economic and environmental benefits.

(4) As the curing time increased, gel filling and particle agglomeration reduced the number of pores in LMGMs, significantly enhancing the internal structure. The dense microstructure is the primary factor for the improvement in strength.

Although many studies have been conducted on the preparation of grouting materials made from shield muck, the properties of muck vary significantly depending on the geological conditions, which, in turn, greatly affect the performance of the grouting materials. This study focuses on the performance of synchronous grouting materials made from loess muck in loess regions, which holds significant practical engineering value. Considering the long-term service performance of engineering structures and the environmental impact of novel grouting materials, it is essential that we further investigate the durability and environmental impact of loess muck grouting materials in future research.

**Author Contributions:** Conceptualization, Z.W. and C.Y.; methodology, Z.W., C.Y. and B.H.; software, Z.W. and F.C.; validation, Z.W., C.Y. and T.Z.; formal analysis, Z.W.; investigation, Z.W. and T.Z.; resources, C.Y.; data curation, C.Y.; writing—original draft preparation, Z.W.; writing—review and editing, C.Y. and F.C.; supervision, B.H.; project administration, C.Y.; funding acquisition, C.Y. and B.H. All authors have read and agreed to the published version of the manuscript.

**Funding:** This research was funded by the National Natural Science Foundation of China (No.52222810) and the China Railway 19th Bureau Group Co., Ltd. (No.19-YHJW-JSFW-2022002).

**Data Availability Statement:** The original contributions presented in the study are included in the article, further inquiries can be directed to the corresponding author.

**Conflicts of Interest:** The authors declare no conflicts of interest.

## References

1. Guo, S.; Wang, B.; Zhang, P.; Wang, S.; Guo, Z.; Hou, X. Influence analysis and relationship evolution between construction parameters and ground settlements induced by shield tunneling under soil-rock mixed-face conditions. *Tunn. Undergr. Space Technol.* **2023**, *134*, 105020. [CrossRef]
2. Tang, C.; Shen, C.; Zhang, J.; Guo, Z. Identification of Safety Risk Factors in Metro Shield Construction. *Buildings* **2024**, *14*, 492. [CrossRef]
3. Wang, X.; Zhao, W.; Wang, Z.; Wang, Z.; Sun, D.; Tang, X. Recycling the discharged soil from EPBS tunnels as a soil conditioner and its rheological behaviors. *J. Clean. Prod.* **2023**, *418*, 138224. [CrossRef]
4. Zhang, J.; Lu, S.; Feng, T.; Yi, B.; Liu, J. Research on reuse of silty fine sand in backfill grouting material and optimization of backfill grouting material proportions. *Tunn. Undergr. Space Technol.* **2022**, *130*, 104751. [CrossRef]
5. Carigi, A.; Saltarin, S.; Di Giovanni, A.; Todaro, C.; Peila, D. Reuse of EPB mucking for concrete production: A laboratory test campaign. *Case Stud. Constr. Mater.* **2023**, *18*, e02187. [CrossRef]
6. Cao, W.; Zhao, J.; Jiang, Z.Y.; Li, Y.Z.; Che, C. Reuse of abandoned shield residues stabilized by a sustainable binder: Assessment of strength, durability, and environmental properties. *Buildings* **2023**, *13*, 738. [CrossRef]
7. Taqa, A.; Al-Ansari, M.; Taha, R.; Senouci, A.; Al-Zubi, G.; Mohsen, M. Performance of concrete mixes containing TBM muck as partial coarse aggregate replacements. *Materials* **2021**, *14*, 6263. [CrossRef]
8. Sharghi, M.; Jeong, H. The Potential of Recycling and Reusing Waste Materials in Underground Construction: A Review of Sustainable Practices and Challenges. *Sustainability* **2024**, *16*, 4889. [CrossRef]
9. Hu, Y.; Yang, D.; Li, S.; Li, H.; Zhang, S.; Hou, Y.; Hu, W.; Zheng, H. Preliminary Study on Preparation of Unfired Bricks Using Filter Cake from Tunnel Muck. *J. Build. Eng.* **2022**, *60*, 105175. [CrossRef]
10. Hong, J.; Chen, Z.; Huang, Y.; Cao, Y.; Geng, S.; Zhang, Y.; Zou, X.; Lu, X. Fabrication and Characterization of Lightweight Aggregate Prepared from Steel Mill Sludge in One Step. *J. Mater. Cycles Waste Manag.* **2022**, *24*, 1072–1082. [CrossRef]
11. Jiao, N.; Wan, X.; Ding, J.; Zhang, X.; Xue, C. Mechanical Properties and Microstructure of Lime-Treated Shield Tunnel Muck Improved with Carbide Slag and Soda Residue. *Constr. Build. Mater.* **2024**, *428*, 136419. [CrossRef]
12. Wang, J.; Fan, Y.; Xiong, X.; Zhao, F. Stabilization of Shield Muck Treated with Calcium Carbide Slag–Fly Ash. *Buildings* **2023**, *13*, 1707. [CrossRef]
13. Guo, W.; Wang, B.; Li, Y.; Mo, S. Status Quo and Prospect of Harmless Disposal and Reclamation of Shield Muck in China. *Tunn. Constr.* **2020**, *40*, 1101.
14. Wu, T.; Gao, Y.; Huang, C.; Jin, A.; Qu, X.; Ji, M.; Zhou, Y.; Li, J. In Situ Resource Reutilization of Earth Pressure Balance (EPB) Shield Muck for the Generation of Novel Synchronous Grouting Materials. *Constr. Build. Mater.* **2024**, *421*, 135737. [CrossRef]
15. Murat, T.; Zhang, L.; Nehdi, M. Development of Sustainable Alkali-Activated Slag Grout for Preplaced Aggregate Concrete. *J. Clean. Prod.* **2020**, *277*, 123488. [CrossRef]
16. Song, W.; Zha, F.; Zhu, Z.; Wang, F. Sulfate Resistance of Novel Alkali-Activated Filling Grout for Shield Tunnels: Comparison with Typical OPC-Based Filling Grout. *J. Mater. Civ. Eng.* **2023**, *35*, 04023472. [CrossRef]
17. Roumeliotis, S.; Lampropoulos, K.; Delegou, E.; Tsilimantou, E.; Keramidas, V.; Bakolas, A.; Moropoulou, A. Enhanced Documentation and Evaluation of Grouting Process, through the Fusion of Non-Destructive Testing and Evaluation Information—The Case Study of the Katholikon of the Monastery of Panagia Varnakova. *Buildings* **2024**, *14*, 814. [CrossRef]
18. Zeng, L.; Zhang, X.; Xie, X.; Zhou, B.; Xu, C.; Lambot, S. Measuring Annular Thickness of Backfill Grouting Behind Shield Tunnel Lining Based on GPR Monitoring and Data Mining. *Autom. Constr.* **2023**, *150*, 104811. [CrossRef]
19. Luo, G.; Xiao, C.; Liu, Y.; Feng, K.; Ren, Q. Research on the Reuse of Discharged Soil from EBP Shield Tunnels in Synchronous Grouting Material. *Adv. Civ. Eng.* **2022**, *2022*, 8102488. [CrossRef]
20. Miltiadou-Fezans, A.; Kalagri, A.; Anagnostopoulou, S. Design and Application of Mortars and Grouts for the Restoration of the Byzantine Church of Panaghia Krena in Chios Island, Greece. *Buildings* **2024**, *14*, 2542. [CrossRef]
21. Zhang, C.; Yang, J.; Fu, J.; Wang, S.; Yin, J.; Xie, Y. Recycling of Discharged Soil from EPB Shield Tunnels as a Sustainable Raw Material for Synchronous Grouting. *J. Clean. Prod.* **2020**, *268*, 121947. [CrossRef]

22. Zhou, S.; Li, X.; Ji, C.; Xiao, J. Back-Fill Grout Experimental Test for Discharged Soils Reuse of the Large-Diameter Size Slurry Shield Tunnel. *KSCE J. Civ. Eng.* **2017**, *21*, 725–733. [CrossRef]
23. Cui, Y.; Tan, Z.; Wang, J.; Shi, Y.; Bai, Z.; Cao, Y. Research on Reuse of Shield Soil Dregs on Synchronous Grouting Materials and Its Application. *Constr. Build. Mater.* **2023**, *408*, 133700. [CrossRef]
24. Ni, Z.; Wang, S.; Zheng, X.; Qi, C. Application of Geopolymer in Synchronous Grouting for Reusing of the Shield Muck in Silty Clay Layer. *Constr. Build. Mater.* **2024**, *419*, 135345. [CrossRef]
25. *GB/T 50123-2019*; Standard for Geotechnical Testing Method. Ministry of Housing and Urban-Rural Development: Beijing, China, 2019.
26. *T/CECS 563-2018*; Technical Specification for Simultaneous Grouting Material in Shield Projects. China Association for Engineering Construction Standardization: Beijing, China, 2018.
27. *JGJ/T 70-2009*; Standard for Test Method of Basic Properties of Construction Mortar. Ministry of Housing and Urban-Rural Development: Beijing, China, 2009.
28. *GB/T 50448-2015*; Technical Code for Application of Cementitious Grout. Ministry of Housing and Urban-Rural Development: Beijing, China, 2015.
29. *JTG E51-2009*; Test Methods of Materials Stabilized with Inorganic Binders for Highway Engineering. Ministry of Transport of the People's Republic of China: Beijing, China, 2009.
30. Song, W.; Zhu, Z.; Pu, S.; Wan, Y.; Huo, W.; Peng, Y. Preparation and Engineering Properties of Alkali-Activated Filling Grouts for Shield Tunnel. *Constr. Build. Mater.* **2022**, *314*, 125620. [CrossRef]
31. Li, Z.; Gao, Y.; Zhang, M.; Zhang, C.; Zhang, J.; Wang, C.; Zhang, N. The Enhancement Effect of Ca-Bentonite on the Working Performance of Red Mud-Slag Based Geopolymeric Grout. *Mater. Chem. Phys.* **2022**, *276*, 125311. [CrossRef]
32. Yin, S.; Zhou, Y.; Wang, L.; Pan, J.; Kou, Y. Setting, Bleeding, and Hardening Strength Properties of Coarse Aggregate Backfill Slurry. *Case Stud. Constr. Mater.* **2022**, *17*, e01667. [CrossRef]
33. Todaro, C.; Pace, F. Elastic Properties of Two-Component Grouts at Short Curing Times: The Role of Bentonite. *Tunn. Undergr. Space Technol.* **2022**, *130*, 104756. [CrossRef]
34. Burris, L.; Kurtis, K. Water-to-Cement Ratio of Calcium Sulfoaluminate Belite Cements: Hydration, Setting Time, and Strength Development. *Cement* **2022**, *8*, 100032. [CrossRef]
35. Sha, F.; Fan, R.; Gu, S.; Xi, M. Strengthening Effect of Sulphoaluminate Cementitious Grouting Material for Water-Bearing Broken Rocky Stratum. *Constr. Build. Mater.* **2023**, *368*, 130390. [CrossRef]
36. Abdalqader, A.; Fayyad, T.; Sonebi, M. Optimization of Fresh Properties, Rheological Parameters and Mechanical Performances of Grouts Containing Bentonite. *Mater. Today Proc.* **2023**, 2214–7853. [CrossRef]
37. Zheng, G.; Huang, J.; Diao, Y.; Ma, A.; Su, Y.; Chen, H. Formulation and Performance of Slow-Setting Cement-Based Grouting Paste (SCGP) for Capsule Grouting Technology Using Orthogonal Test. *Constr. Build. Mater.* **2021**, *302*, 124204. [CrossRef]
38. Li, W.; Zhang, Q.; Li, L.; Li, Y.; Zhang, H.; Lu, L. Investigation on Water and Fertilizer Retention Properties of Hydrated Sulphoaluminate Cement Pastes Modified by Bentonite for Porous Ecological Concrete. *Case Stud. Constr. Mater.* **2023**, *18*, e01967. [CrossRef]
39. Xu, J.; Xiao, C.; Wu, H.; Kang, X. Reuse of Excavated Clayey Silt in Cement–Fly Ash–Bentonite Hybrid Back-Fill Grouting During Shield Tunneling. *Sustainability* **2020**, *12*, 1017. [CrossRef]
40. Huynh, P.T.; Ogawa, Y.; Kawai, K.; Bui, P.T. Effect of Cement Type and Water-to-Binder Ratio on k-Value of Low-Calcium Fly Ash for Concrete Compressive Strength. *J. Mater. Civ. Eng.* **2023**, *35*, 04023427. [CrossRef]
41. Rudić, O.; Ukrainczyk, N.; Krüger, M.; Tritthart, J.; Juhart, J. Efficiency of Limestone in Clinker-Reduced Binders: Consideration of Water-Binder Ratio, Capillary Porosity and Compressive Strength. *Constr. Build. Mater.* **2023**, *386*, 131594. [CrossRef]
42. Nag, M.; Labira, D.; Shimaoka, T.; Nakayama, H.; Komiya, T. Utilization of Size-Fractionated Pozzolanic Bottom Ash to Immobilize Heavy Metals in MSW Incinerator Fly Ash. *J. Environ. Chem. Eng.* **2023**, *11*, 110394. [CrossRef]
43. Ran, B.; Omikrine-Metalssi, O.; Fen-Chong, T.; Dangla, P.; Li, K. Pore Crystallization and Expansion of Cement Pastes in Sulfate Solutions with and Without Chlorides. *Cem. Concr. Res.* **2023**, *166*, 107099. [CrossRef]
44. Rocha, J.; Filho, R. Microstructure, Hydration Process, and Compressive Strength Assessment of Ternary Mixtures Containing Portland Cement, Recycled Concrete Powder, and Metakaolin. *J. Clean. Prod.* **2024**, *434*, 140085. [CrossRef]
45. Ma, X.; He, T.; Xu, Y.; Yang, R.; Sun, Y. Hydration Reaction and Compressive Strength of Small Amount of Silica Fume on Cement-Fly Ash Matrix. *Case Stud. Constr. Mater.* **2022**, *16*, e00989. [CrossRef]
46. Du, S.; Zhang, Y.; Zhang, J.; Selyutina, N.; Smirnov, I.; Ma, G.; Zhang, X.; Li, B.; Miao, Y.; Liu, Y.; et al. Study on Pore Characteristics of Recycled Aggregate Concrete Mixed with Glazed Hollow Beads at High Temperatures Based on 3-D Reconstruction of Computed Tomography Images. *Constr. Build. Mater.* **2022**, *323*, 126564. [CrossRef]
47. Song, W.; Zhu, Z.; Pu, S.; Wan, Y.; Huo, W.; Song, S.; Zhang, J.; Yao, K.; Hu, L. Efficient Use of Steel Slag in Alkali-Activated Fly Ash-Steel Slag-Ground Granulated Blast Furnace Slag Ternary Blends. *Constr. Build. Mater.* **2020**, *259*, 119814. [CrossRef]


**Disclaimer/Publisher's Note:** The statements, opinions and data contained in all publications are solely those of the individual author(s) and contributor(s) and not of MDPI and/or the editor(s). MDPI and/or the editor(s) disclaim responsibility for any injury to people or property resulting from any ideas, methods, instructions or products referred to in the content.